Cell Reports
Physical Science

CellPress
OPEN ACCESS

Article

Dynamic interplays between three redox cofactors in a DNA photolyase revealed by spectral decomposition

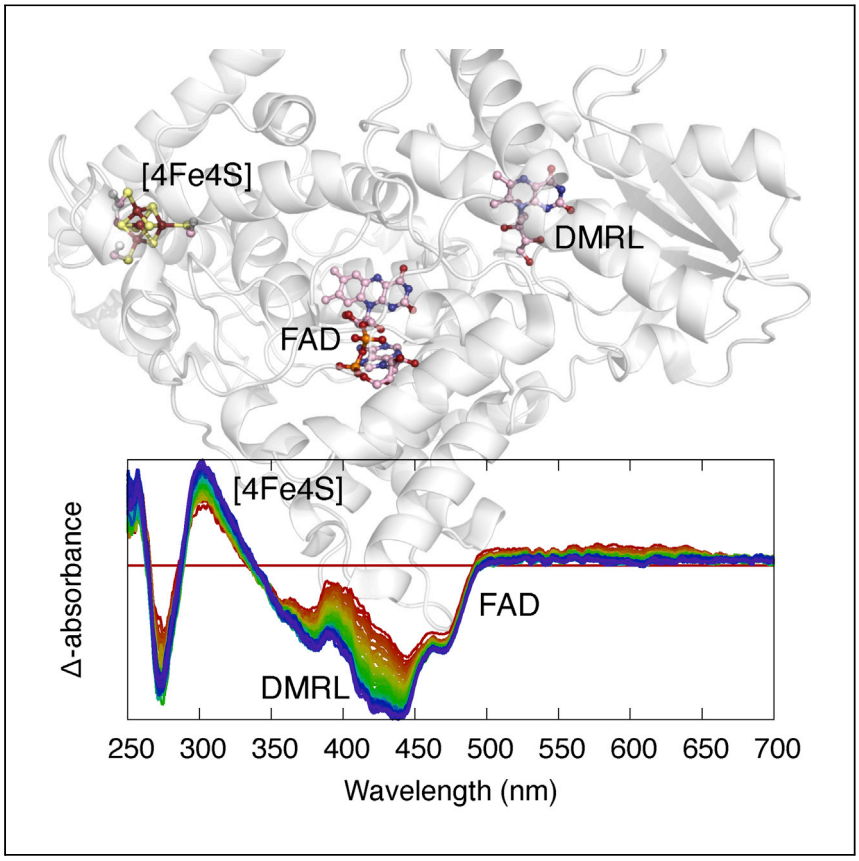

Here, Ren et al. develop a mathematical procedure to analyze a large collection of spectroscopic data. By dissecting concurrent spectral changes, the authors reveal the cooperation between three prosthetic cofactors that work together to manage potential risk in a DNA repair enzyme.

Zhong Ren, Weijia Kang, Semini Gunawardana, ..., Norbert Krauß, Tilman Lamparter, Xiaojing Yang

zren@uic.edu (Z.R.)
xiaojing@uic.edu (X.Y.)

Highlights

Spectral features of three cofactors in a DNA repair photolyase are decomposed

An interdependent redox network between cofactors is revealed

The ribolumazine cofactor plays a photoprotective role under intense light

An iron-sulfur cluster acts as a transient electron cache to balance electron flow

Ren et al., Cell Reports Physical Science 4, 101297
March 15, 2023
https://doi.org/10.1016/j.xcrp.2023.101297

Cell Reports
Physical Science

CellPress
OPEN ACCESS

Article

Dynamic interplays between three redox cofactors in a DNA photolyase revealed by spectral decomposition

Zhong Ren,[1,4,*] Weijia Kang,[1] Semini Gunawardana,[1] Kalinga Bowatte,[1] Katharina Thoulass,[2] Gero Kaeser,[2] Norbert Krauß,[2] Tilman Lamparter,[2] and Xiaojing Yang[1,3,*]

SUMMARY

DNA repair catalyzed by photolyases is accomplished by a light-dependent electron transfer event from a fully reduced flavin adenine dinucleotide to a DNA lesion site. Prokaryotic DNA photolyase, PhrB, possesses a ribolumazine cofactor and a four-iron-four-sulfur cluster in addition to the catalytic flavin, but their functional roles are poorly understood. Here, we employ time-resolved absorption spectroscopy to probe light-induced responses in both solution and single crystals of PhrB. We jointly analyze a large collection of light-induced difference spectra from the wild-type and mutant PhrB obtained under different light and redox conditions. By applying singular value decomposition to 159 time series, we dissect light-induced spectral changes and examine the dynamic interplay between three cofactors. Our findings suggest that these cofactors form an interdependent redox network to coordinate light-induced redox responses. We propose that the ribolumazine cofactor serves as a photoprotective pigment under intense light or prolonged illumination, while the iron-sulfur cluster acts as a transient electron cache to maintain balance between two otherwise independent photoreactions of the flavin and ribolumazine.

INTRODUCTION

DNA lesions caused by ultraviolet (UV) irradiation are detrimental to living organisms. If not repaired, these photochemical modifications would alter DNA replication and transcription, leading to high mutation rates and genome instability. UV-induced DNA damages include two major types of photoproducts, namely cyclobutane pyrimidine dimers and pyrimidine-pyrimidone (6-4) photoproducts. Both involve cross-linking of adjacent thymine bases.[1] Among many DNA repair mechanisms, photolyases are light-dependent flavoenzymes that directly revert DNA lesions. This photoreactivation process utilizes violet and blue light that often comes with UV radiation.[2] A repair-competent photolyase requires a fully reduced flavin adenine dinucleotide (FAD) cofactor, and its activation may or may not depend on light *in vivo*.[3] Upon photoexcitation of the fully reduced hydroquinone $FADH^-$, a DNA repair reaction takes place when an electron is transferred from the flavin to the DNA lesion site.[4]

Many photolyases acquire an additional cofactor(s) that does not directly participate in the DNA repair reaction. They are thought to function as antenna pigments. Recently, a distinct class of bacterial photolyases has been found to contain a four-iron-four-sulfur cluster ([4Fe4S]).[5–8] PhrB from *Agrobacterium fabrum* is a

[1]Department of Chemistry, University of Illinois Chicago, Chicago, IL, USA

[2]Botanical Institute, Karlsruhe Institute of Technology, Karlsruhe, Germany

[3]Department of Ophthalmology and Vision Sciences, University of Illinois Chicago, Chicago, IL, USA

[4]Lead contact

*Correspondence: zren@uic.edu (Z.R.), xiaojing@uic.edu (X.Y.)

https://doi.org/10.1016/j.xcrp.2023.101297

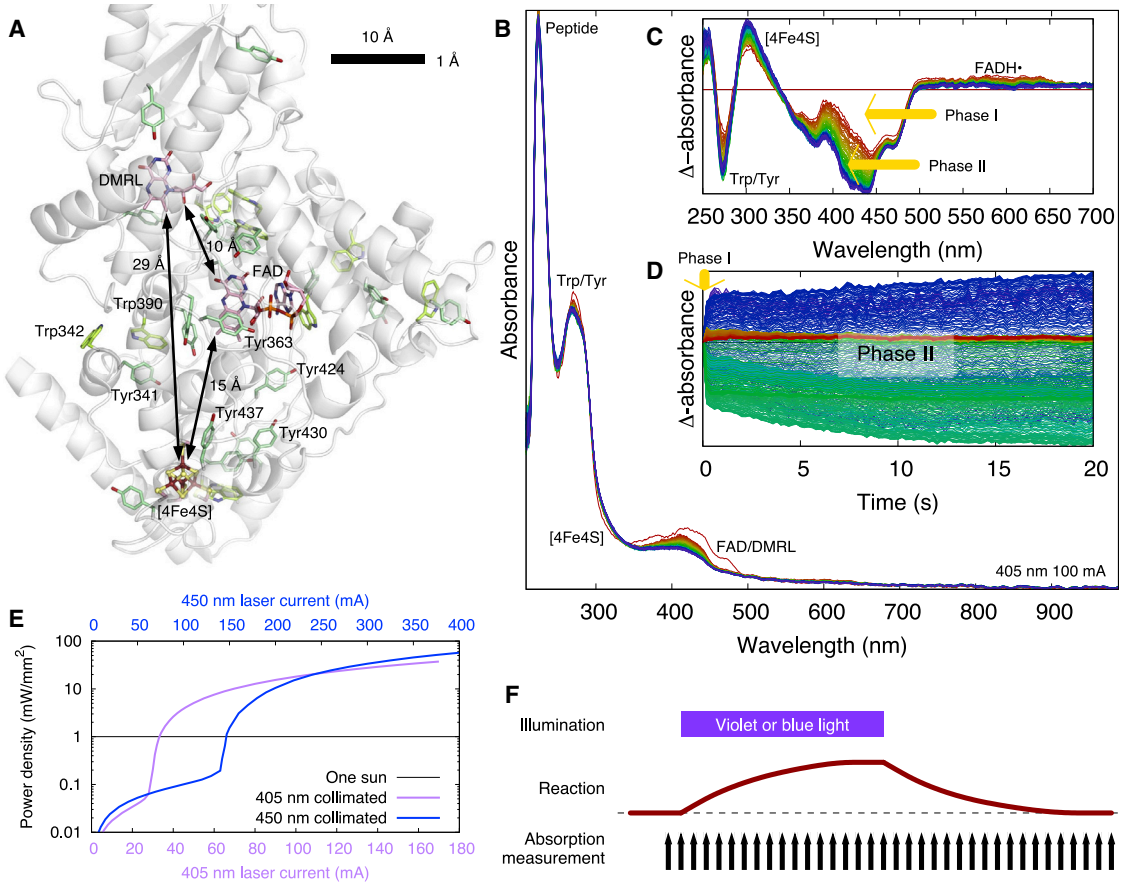

Figure 1. Three cofactors in the PhrB structure and time course of light-induced absorption spectra

(A) Disposition of three redox cofactors in PhrB. The protein is rendered in white ribbon. FAD, DMRL, and the Cys anchors of the [4Fe4S] cluster are in pink. Trp and Tyr residues are in different shades of green. A scale bar is placed at the upper right corner.

(B) A time series of UV-visible absorption spectra of wild-type PhrB solution follows light-induced spectral changes. The spectra are colored from red to blue in equal spacing during a 20-s illumination of violet light at 405 ± 5 nm. Strong bands in mid-UV < 300 nm arise from the absorption of peptide bonds and Trp/Tyr residues shown in (A). Absorption bands in the near-UV and blue regions are attributed to light-induced changes in three redox pigments shown in (A). However, contributions from three cofactors are entangled in the raw measurements that would require a numerical deconvolution for clear interpretation.

(C) Difference spectra. The first spectrum taken before the illumination was used as a reference and subtracted from all subsequent spectra (F). Absorption loss in the near-UV and blue regions proceeds in two phases. Phase I is completed within a fraction of a second, while phase II develops in seconds.

(D) Temporal traces of absorbance changes are colored from purple to red according to wavelengths in the range of 250–700 nm.

(E) Power density of illumination. The power density as a function of the electric current setting of the laser diodes was measured with an optical power meter (Thorlabs). See experimental procedures supplemental experimental proceduresfor details.

(F) Experimental timing. The first absorption spectrum was measured before the illumination started, which serves as a dark reference. Absorption spectra were repeatedly measured with equal spacing during illumination of violet and blue light at 405 and 450 nm, respectively. Absorption spectra were also measured after an illumination during dark reversion.

representative [4Fe4S]-containing DNA photolyase that has been characterized by X-ray crystallography (Figure S1) and shown to repair (6-4) photoproducts.[9] PhrB adopts a typical U-shaped FAD conformation, which is solvent-accessible at the active site in the absence of the DNA substrate (Figure S2). Compared with undamaged single-stranded DNA, PhrB confers a nearly 2,000-fold higher binding affinity for single-stranded DNA substrates carrying a damaged (6-4) photoproduct.[10] In addition to the catalytic FAD, PhrB harbors a second chromophore, 6,7-dimethyl-8-ribityllumazine (DMRL), deeply embedded in the N-terminal domain (Figures 1A and S1). The ribolumazine DMRL is a riboflavin precursor in the biosynthetic

pathway.[11,12] Since DMRL assumes the same location as the antenna pigments, such as 8-hydroxy-7,8-didemethyl-5-deazariboflavin (8-HDF), in other photolyases (Figure S3), it has been proposed that DMRL functions as a similar light-harvesting antenna pigment.[13] PhrB features a third inorganic cofactor, [4Fe4S], which is embedded in the C-terminal domain and stabilized by four Cys residues (Figures 1A and S1). While the catalytic role of FAD is well established for photolyases, the functional roles of DMRL and [4Fe4S] are not clear, although possible excitation energy transfer from DMRL to FAD has been suggested.[14]

In this work, we carry out a global analysis on a large collection of light-induced difference spectra in 159 time series obtained from single crystals and solution samples of PhrB. Using singular value decomposition (SVD), we deconvolute the mixed signals in the concurrent and overlapping spectral changes according to the characteristic spectral features of each cofactor so that their responses to different experimental perturbations can be examined and their dependency on or relationship with one another can be shown as their correlations. Our findings suggest that the three redox cofactors of PhrB form an intricate network within the protein moiety, where [4Fe4S] is coupled to both FAD and DMRL. Such redox network not only balances electrons between two photoreactions of FAD and DMRL, but also is likely to play an important role in safeguarding production of the highly reactive, fully reduced flavin under a variety of light conditions.

RESULTS AND DISCUSSION

Overview of spectroscopic experiments

The absorption spectra of FAD, DMRL, and [4Fe4S] in PhrB overlap significantly in the mid-UV, near-UV to violet, and blue light regions (Figure 1B). Each cofactor also features multiple redox states during the processes of photoreaction and dark reversion. It is often difficult to track simultaneous spectral changes as these cofactors transition from one state to another. Given that each redox state of a specific cofactor has a distinct spectral signature (Figure S4), it is possible to dissect light-induced spectral changes using analytical methods. To follow and dissect the concurrent photochemical events in three cofactors as well as possible redox changes in the protein, we chose to use continuous-wave (CW) lasers as a pump light to record the time course of spectral changes that span tens of seconds (experimental procedures; Figures 1E and 1F). This approach contrasts with pulsed lasers with faster time resolution in ultrafast time-resolved experiments aimed to probe the photochemical events of a specific cofactor.[15,16] To examine possible interplay between cofactors, we illuminated the wild-type and mutant PhrB at wavelengths of 405 and 450 nm, where the violet light at 405 nm is near the peak absorption of DMRL, but in an absorption minimum of the fully oxidized FAD, and the blue light at 450 nm is at the peak absorption of FAD, but at the foothill of DMRL absorption (Figures S4A and S4B). Therefore, these wavelengths selectively excite DMRL or FAD more than the other. To explore whether the ambient redox conditions affect the photoreactions, we also recorded the light-induced spectral changes and dark reversion processes from the PhrB samples with and without the reducing agent tris(2-carboxyethyl)phosphine (TCEP) or dithiothreitol (DTT). In addition, we performed power titration experiments in which light intensity was exploited as a rate-limiting reactant to probe photoproduct species under both low and high light conditions. To support our crystallographic studies, we also conducted the spectroscopic measurements on PhrB single crystals. Altogether, we obtained 15,465 absorption spectra in 159 time series from both single crystals and solution samples (Figure 1F).

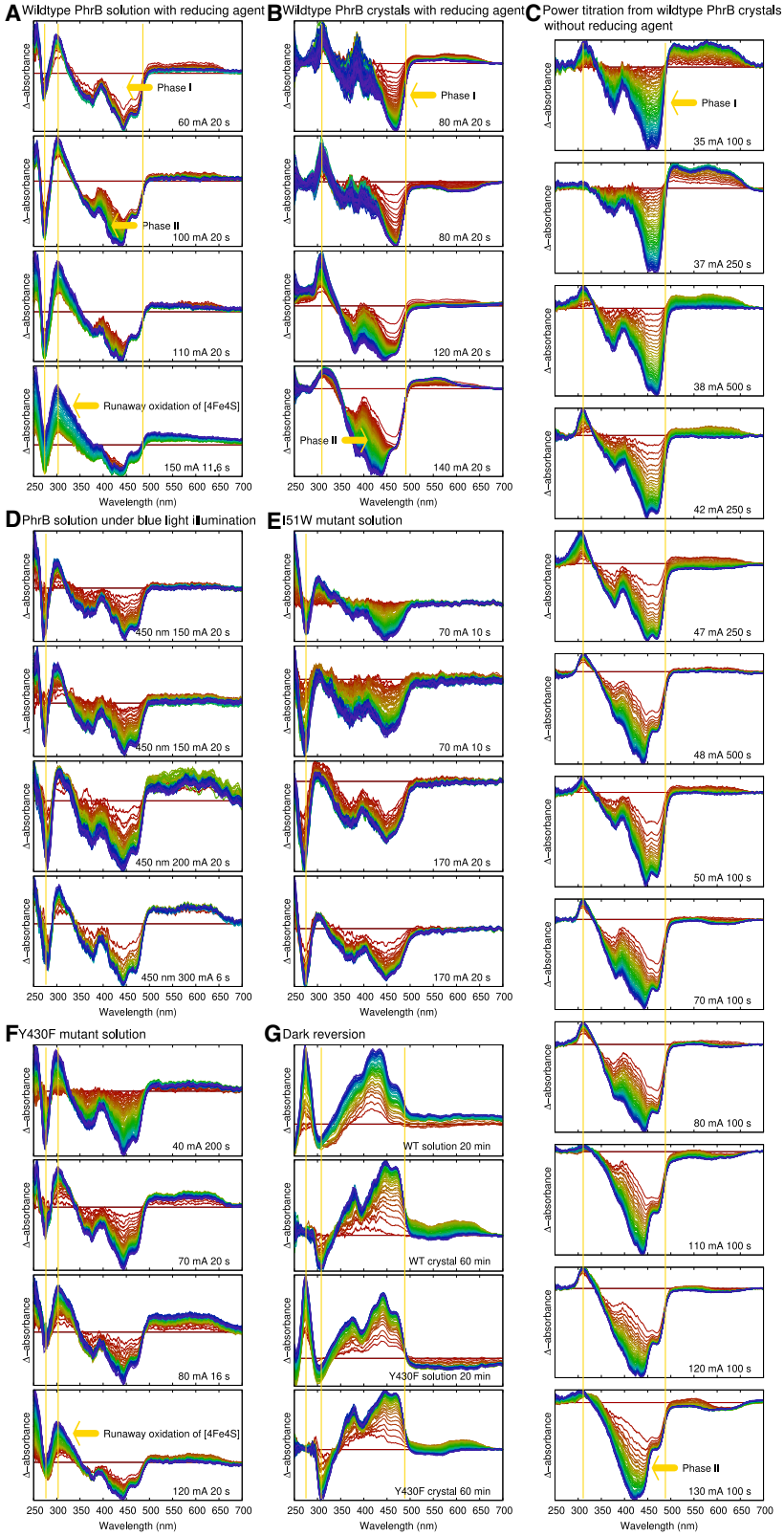
A Wildtype PhrB solution with reducing agent
Phase I
60 mA 20 s
Phase II
100 mA 20 s
110 mA 20 s
Runaway oxidation of [4Fe4S]
150 mA 11.6 s
B Wildtype PhrB crystals with reducing agent
Phase I
80 mA 20 s
80 mA 20 s
120 mA 20 s
Phase II
140 mA 20 s
C Power titration from wildtype PhrB crystals without reducing agent
Phase I
35 mA 100 s
37 mA 250 s
38 mA 500 s
42 mA 250 s
D PhrB solution under blue light illumination
450 nm 150 mA 20 s
450 nm 150 mA 20 s
450 nm 200 mA 20 s
450 nm 300 mA 6 s
E I51W mutant solution
70 mA 10 s
70 mA 10 s
170 mA 20 s
170 mA 20 s
47 mA 250 s
48 mA 500 s
50 mA 100 s
70 mA 100 s
F Y430F mutant solution
40 mA 200 s
70 mA 20 s
80 mA 16 s
Runaway oxidation of [4Fe4S]
120 mA 20 s
G Dark reversion
WT solution 20 min
WT crystal 60 min
Y430F solution 20 min
Y430F crystal 60 min
80 mA 100 s
110 mA 100 s
120 mA 100 s
Phase II
130 mA 100 s
Δ–absorbance
250 300 350 400 450 500 550 600 650 700
Wavelength (nm)

Figure 2. Representative difference absorption spectra of PhrB under various experimental conditions

Each part displays a time series of difference spectra from red to blue with equal spacing during the individually marked illumination periods. The illumination wavelength is 405 ± 5 nm except as marked otherwise in (D). The electric current through the laser diode determines the power density of the illumination (Figure 1E).

(A) Wild-type PhrB solution. Each time series is measured from a solution drop of 1 μL with the reducing agent of 5 mM TCEP. The biphasic photoreduction of FAD and DMRL is clearly visible. The characteristic sharp edge of absorption loss at 485 nm is a signature of FAD reduction (Figure S4A, black curve). A sharp loss of absorption at 275 nm with a full width at half-maximum (FWHM) of 20 nm is observed only from solution samples.

(B) Wild-type PhrB crystal. Each time series is measured from a single crystal grown with 5 mM TCEP. The biphasic photoreduction is identical to that in solution (A). However, no absorption loss at 275 nm is observed in crystals.

(C) Power titration measurements from wild-type PhrB crystals. No reducing agent was added. The photoreduction of FAD in phase I develops in low light.[8,10] It completes quickly in high light. Phase II of photoreduction due to DMRL starts and develops in high light. The broadband at longer wavelengths, >485 nm, characteristic of the neutral radical semiquinone FADH• (Figure S4A, blue curve)[39] exhibits a complex time course. The absorption gain centered at 308 nm is not consistent from one time series to another. When the power density of the illumination is taken into account, these time series are converted to more consistent absorbance changes in the domain of illumination dose except for the absorption band of [4Fe4S] at 308 nm (Figure S7).

(D) Blue pump light at 450 nm. Wild-type PhrB solution drops with reducing agent are illuminated by 450 ± 5 nm light. Phase II of the photoreduction is not observed.

(E) I51W mutant solution. PhrB mutant I51W carries no DMRL cofactor.[14] Phase II of the photoreduction is not observed.

(F) Y430F mutant solution. Y430F solution is illuminated without reducing agent.

(G) Dark reversion. Each time series is measured from a wild-type or mutant solution drop or a single crystal after the illumination is over. All spectral changes are fully reversible in the dark, including both phases of photoreduction and other absorption gain and loss at 308 and 275 nm, both in solution and in crystal.

Under low-power violet light at 405 nm, we observe significant bleaching in the near-UV and blue regions as previously reported.[8,10] Remarkably, a second phase of absorption loss starts to appear in the same region and develops further under more intense or prolonged illumination in a power titration experiment (Figures 1B and 2). The solution and crystal samples of PhrB show similar biphasic behavior in the blue region, except that a sharp absorption loss centered around 275 nm exclusively occurs in PhrB solution samples, likely associated with redox and/or conformational changes in the Trp and Tyr residues (Figures 2A and 2B). However, the phase II of absorption loss is not prominent under blue light illumination at 450 nm nor in the single mutant I51W, where the second cofactor DMRL is knocked out (Figures 2D and 2E). The effect of a reducing agent is not immediately obvious (Figures 2B and 2C) and will require more quantitative analysis (see below). Interestingly, an additional absorption gain centered around 308 nm exhibits no consistent trend over a wide range of power densities (Figure 2), except that this peak seems to gradually rise and broaden under intense violet light (Figures 2A and 2F). Furthermore, all spectral changes are fully reversible in tens of minutes to hours following the withdrawal of the excitation light (Figure 2G). Taken together, a first glance at these time series suggests that the photoreaction of PhrB is more complicated than the simple FAD photoreduction, and the light-induced responses clearly involve other cofactors, which calls for an in-depth global analysis to determine the functional roles and possible interplays between different cofactors in PhrB.

Global analysis of difference absorption spectra

To address the complexity arising from significant spectral overlaps of multiple cofactors, we applied SVD to jointly analyze 159 time series from PhrB obtained under various experimental conditions. SVD, widely used for signal processing, including

data analysis in time-resolved spectroscopy, is particularly useful for extracting subtle signals from noisy data.[17,18] SVD, together with the posterior procedures described below, is based on a set of numerical techniques recently developed to tackle heterogeneous structural signals in dynamic crystallography (supplemental experimental procedures).[19–21] Here, we present the global analysis scheme to compare a large collection of spectra.

As the numerical procedure of SVD guarantees, the major differences among these spectra stand out as indicated by the larger singular values, while the minor differences and inconsistent noises are associated with the smaller singular values (supplemental experimental procedures). Simply put, each experimentally measured spectrum $A(\lambda, t)$ can be considered as a linear combination of a few major spectral components after SVD, such as $A(\lambda, t) = c_1(t)U_1(\lambda) + c_2(t)U_2(\lambda) + \ldots$, where A represents light-induced difference absorbance as a function of the wavelength λ and time t. In SVD, a large collection of spectral data is decomposed into time-dependent but wavelength-independent coefficients $c_k(t)$ (Figure 4) and time-independent components $U_k(\lambda)$ (Figure 3). These components are ranked according to their corresponding singular values. The spectral components $U_k(\lambda)$ are also independent of the experimental conditions, including the wavelength of excitation light, power density, temperature, redox condition, crystal or solution, wild type or mutant, and forward or backward reaction. Most of the minor spectral components can be safely discarded, as they likely contain noise only, while the signals are captured by a small number of the top components. As a result, a time series of spectral changes is represented by a multidimensional temporal trace determined by the time-dependent coefficient set $c_1(t)$, $c_2(t)$, …. Meanwhile, the coefficient plots can be used to examine the correlation and origins of the corresponding spectral signals (Figure 4).

It is well known that the decomposed components directly from SVD are often difficult to comprehend because they are only the result of a mathematical decomposition and may or may not carry any specific chemical or physical meaning. To extract chemically sensible spectral features associated with specific cofactors and reactions, a rotation procedure[19–21] was performed in a multidimensional Euclidian space of $c_1(t)$, $c_2(t)$, …, that was established by SVD (supplemental experimental procedures). As a result, characteristic spectral changes arising from distinct chemical events such as FAD and DMRL photoreduction or [4Fe4S] oxidation, and even those from redox and/or conformational changes in the protein, could be effectively deconvoluted into different components (Figure 3). If the spectral features attributed to two or more cofactors could not be isolated from one another, it is reasonable to infer that the corresponding cofactors were coupled in their responses within the achievable time resolution in our experiments (supplemental experimental procedures).

Given that the rate-limiting step in a CW laser experiment is largely governed by the incident photon flux, the excitation power density was employed as a variable to probe the photoreactions on different time scales. For example, phase II of the absorption loss could be detected much sooner using high-power illumination (Figure 2C). To account for the effects arising from differences in optical thickness of the sample and intensity of the pump light, we also subjected all spectral data to amplitude and temporal normalization in our joint analysis (supplemental experimental procedures). The amplitude normalization removed any effects arising from a wide range of optical thicknesses due to variations in crystal size and protein concentration in solution (supplemental experimental procedures; Figures S5 and S6). The temporal normalization resulted in a time unit equivalent to 1 s in a specific

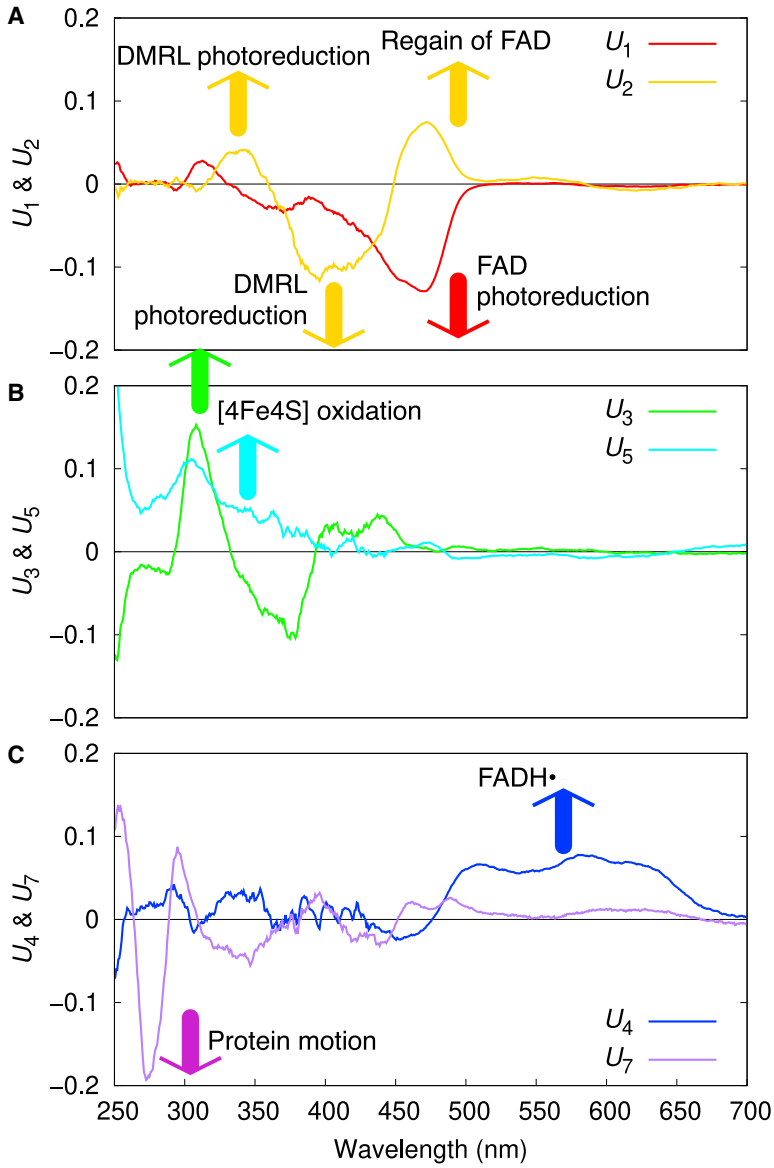

Figure 3. Spectral components of PhrB

Spectral components derived from SVD analysis (supplemental experimental procedures) are colored differently.

(A) The first component $U_1(\lambda)$ features the characteristic sharp edge of absorption loss at 485 nm with FWHM of 10 nm, a signature of the FAD reduction (Figure S4A, black curve). $U_2(\lambda)$ features the positive edge at the same position that signifies the regain of the fully oxidized FAD. A pair of an absorption loss from 375 to 450 nm and an absorption gain at 345 nm with FWHM of 40 nm in $U_2(\lambda)$ matches well with the observed absorption changes of a small lumazine protein upon blue-light illumination when DMRL is photoreduced (Figure S4B, black curve).[22]

(B) The main feature of $U_3(\lambda)$ is a sharp absorption gain at 308 nm with FWHM of 25 nm combined with an absorption loss at 350–390 nm. $U_5(\lambda)$ carries broad absorption gains in near UV, <400 nm. These spectral features are attributed to the oxidation of [4Fe4S] (Figure S14).

(C) $U_4(\lambda)$ is the only component that features the broad absorption gain at 485–655 nm in the visible wavelength range from cyan to green, yellow, and red, which is characteristic of the neutral radical semiquinone FADH• (Figure S4A, blue and gray curves).[39] $U_7(\lambda)$ features a sharp absorption loss at 275 nm with FWHM of 20 nm. This characteristic absorption band of Trp and Tyr residues indicates motions in the protein or redox changes to these residues. The other spectral components among the top 10 are also significant, but mostly carry systematic errors of the experiments.

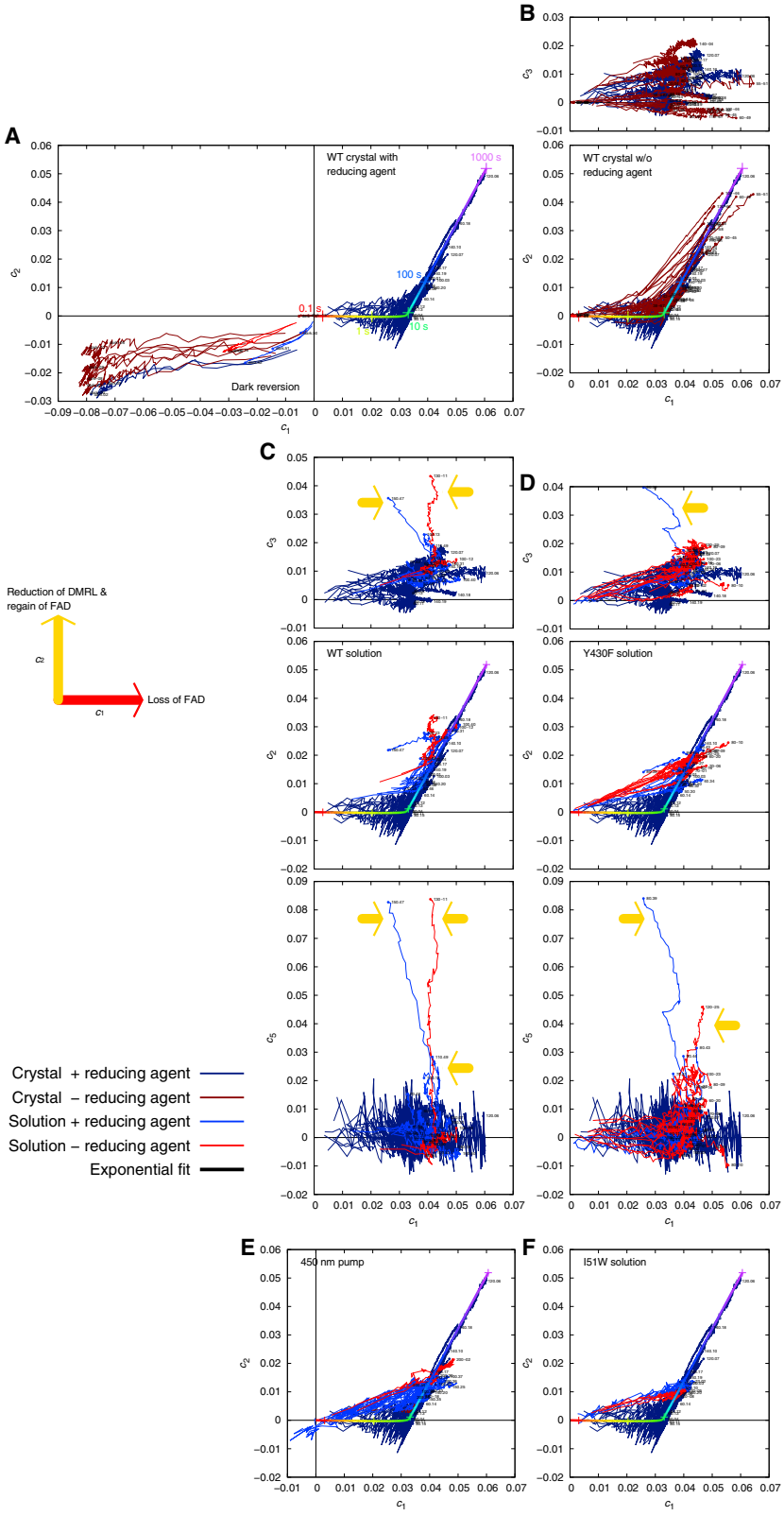
A
WT crystal with reducing agent
1000 s
100 s
10 s
1 s
0.1 s
Dark reversion
B
WT crystal w/o reducing agent
C
WT solution
D
Y430F solution
E
450 nm pump
F
I51W solution
Reduction of DMRL & regain of FAD
Loss of FAD
Crystal + reducing agent
Crystal − reducing agent
Solution + reducing agent
Solution − reducing agent
Exponential fit

Figure 4. Reaction trajectories of PhrB

Correlations between the time-dependent coefficients $c_1(t)$, $c_2(t)$, $c_3(t)$, and $c_5(t)$ are plotted in separate parts for comparison. Each trace represents a time series that starts from the origin and ends with a dot. Time traces collected with a reducing agent are plotted in blue colors, and those without a reducing agent are in red colors. Time traces collected from solution samples are in lighter blue and red. Those from single crystals are in darker blue and red.

(A) Crystals of wild-type PhrB grown with a reducing agent of TCEP or DTT at 5 mM. The first spectral component increases at the beginning of a time series. After the sharp turn, the second component increases faster than the first does. Such a common temporal trajectory after the normalization clearly shows that the photoreductions of FAD and DMRL proceed in two distinct phases (supplemental experimental procedures; Figure S6). The result of an exponential fitting of these coefficients is plotted as a thick curve. The normalized time is color coded from 0.1 to 1,000 time units. A time unit corresponds to 1 s in one of the time series derived from 405-nm illumination at 100 mA current setting (Figure 1E). Time series during the dark reversion (Figure 2G) also start from the origin but go toward negative c_1 and c_2.

(B) Crystals of wild-type PhrB grown without a reducing agent. The time series measured without a reducing agent in dark red are superimposed over those with a reducing agent in dark blue (A). Most of them agree well. But some of the time series in dark red show fewer sharp turns between two phases, which indicates that the photoreduction enters phase II sooner without a reducing agent. $c_3(t)$ without a reducing agent diverges more than those with a reducing agent.

(C) Wild-type PhrB in solution. Time series derived from solution with and without a reducing agent in lighter blue and red, respectively, are superimposed over those from crystal with a reducing agent in dark blue (A). Phase I of the time series seems to carry a small baseline of c_2, which may indicate a small fraction of the reduced DMRL at the beginning of the illumination. Several time series under high-power illumination turn around and show some regaining of the fully oxidized FAD. $c_3(t)$ and $c_5(t)$ of these time series run far away from those in the usual time series, indicating extended oxidation of [4Fe4S] as marked by yellow arrows (Figures 2A and S10).

(D) PhrB mutant Y430F in solution. Time series from solution Y430F mutant in lighter blue and red are superimposed over those from crystal with a reducing agent in dark blue (A). A shortcut between two phases in a straight line bypasses the sharp turn in dark blue. However, some time series derived from high-power illumination turn around to regain some of the fully oxidized FAD. $c_3(t)$ and $c_5(t)$ of these time series also show extended oxidation of [4Fe4S] as marked by yellow arrows (Figures 2F and S13).

(E) Blue pump light at 450 nm. Time series in lighter blue and red derived from 450 nm illumination are superimposed over those from crystal with a reducing agent in dark blue (A). Coefficient c_2 does not reach the same level as that under violet light illumination, because of less DMRL absorption at 450 nm (Figures 2D, S4B, and S11). The photoreaction proceeds in a straight line.

(F) PhrB mutant I51W without DMRL in solution. Time series from the solution I51W mutant in lighter blue and red are superimposed over those from crystal with a reducing agent in dark blue (A). Phase II is absent (Figures 2E and S12).

time series derived from a wild-type crystal. Only the relative rates between different reaction phases are discussed (Figure S6). We also replace the variable time with illumination dose, since the power density of the pump laser had been measured (Figure 1E). Taking the power density into consideration, absorbance changes measured under drastically different illumination intensity and duration (Figure 2C) largely agreed with one another as a function of illumination dose (Figure S7).

These analytical protocols enabled us to examine the spectral components and their time traces in 159 time series of difference absorption spectra in a multidimensional space (Figure S8). Our findings revealed how three redox cofactors work together to achieve coordinated light responses of PhrB under a variety of experimental conditions (Figures S9–S13).

Biphasic responses and coupling between FAD and DMRL

The raw difference spectra obtained under violet light at 405 nm clearly show that light-induced spectral changes proceed in two distinct phases in wild-type PhrB solution and single crystals, both with the presence of a reducing agent (Figures 1B, 1C, 1D, 2A, and 2B). This biphasic response is characterized by an early rise in the

coefficient $c_1(t)$ corresponding to the first spectral component $U_1(\lambda)$ from SVD that features an absorption loss with a sharp edge at 485 nm (Figure 3A). This rapid phase I is characteristic of the loss of the fully oxidized species of FAD due to its photoreduction (Figure S4A). The second phase is much slower, and the coefficient $c_2(t)$ increases at a time constant 70 times greater than that of $c_1(t)$ in phase I (Figures 4A, S6B, S6D, and S6E). In addition to a positive sharp edge at 485 nm characteristic of the fully oxidized FAD, the second component $U_2(\lambda)$ also reveals an absorption gain at 345 nm and a broad loss around 375–450 nm, attributed to the DMRL photoreduction because they agree quite well with the light-induced spectral changes in the wild-type protein LumP incorporated with the ribolumazine cofactor DMRL (Figure S4B).[22] The observation that these spectral features are present in the same SVD component $U_2(\lambda)$ suggests that the DMRL photoreduction and flavin oxidation are directly coupled, likely via an electron transfer event from the flavin to DMRL, at least within the sub-second time resolution achieved in this work (Figure 5, steps 2, 6, and 7). Consistently, the $U_2(\lambda)$ component is relatively small in the time series obtained under blue light illumination at 450 nm (Figures 2D, 4E, and S11), where the DMRL absorption is minimal (Figure S4B), and in the I51W mutant (Figures 2E, 4F, and S12), where DMRL is removed from PhrB.[14]

Similar spectral changes have been observed for PhrB in solution (Figures 2A, 4C, and S10). One exception is that a sharp absorption loss at 275 nm featured in the component $U_7(\lambda)$ (Figure 3C) is observed only from solution samples, as all the time series derived from crystals feature a nearly constant $c_7(t) \approx 0$ (Figure S8B, bottom row), which suggests possible involvement of Trp/Tyr motions or redox changes that may be prohibited in the crystal lattice. Under aerobic conditions, the time series of dark reversion spanning tens of minutes to hours show spontaneous oxidization of flavin in the absence of light in both solution and crystal samples (Figures 2G, 4A, S5, and S8B, middle column). However, the dark reversion appears to proceed in a single phase with transient accumulation of the semi-reduced flavin species FADH•. This is evidenced by the rise and fall of the coefficient $c_4(t)$ (Figure S8B, second last row) and the corresponding spectral component $U_4(\lambda)$ featuring the broadband absorption gain at 485–655 nm, which is characteristic of the semiquinone (Figures 3C and S4A).

Taken together, our data suggest that the photoreduction of DMRL and oxidation of FAD are highly coupled in the same protein of PhrB. This coupling is more prominent under high light conditions that excite DMRL (Figure 5). FAD and DMRL are apart by ~10 Å in the PhrB structure (Figure 1A). It is not known whether this coupling involves any mediators in between. Most noticeably, Tyr399 between FAD and DMRL could play a role in electron transfer. A detailed study on these electron transfer events requires faster time resolution beyond the scope of this work. It is plausible that the DMRL photoreduction offers some regulatory function, such as protection from high-light or prolonged illumination by actively reverting the highly energetic flavin to its fully oxidized, catalytically incompetent species, especially in the absence of DNA lesions.

Iron-sulfur cluster as an electron cache

Our analysis has revealed two highly variable spectral components. Specifically, the third spectral component $U_3(\lambda)$ features a sharp absorption gain at 308 nm and a loss around 375 nm (Figure 3B), which has also been observed previously.[10] In contrast to the highly reproducible biphasic behavior of $U_1(\lambda)$ and $U_2(\lambda)$, the coefficient $c_3(t)$ appears to diverge significantly farther along the reaction course, and in some time series it even heads toward the negative regime (Figures 4B, 4C, and 4D).

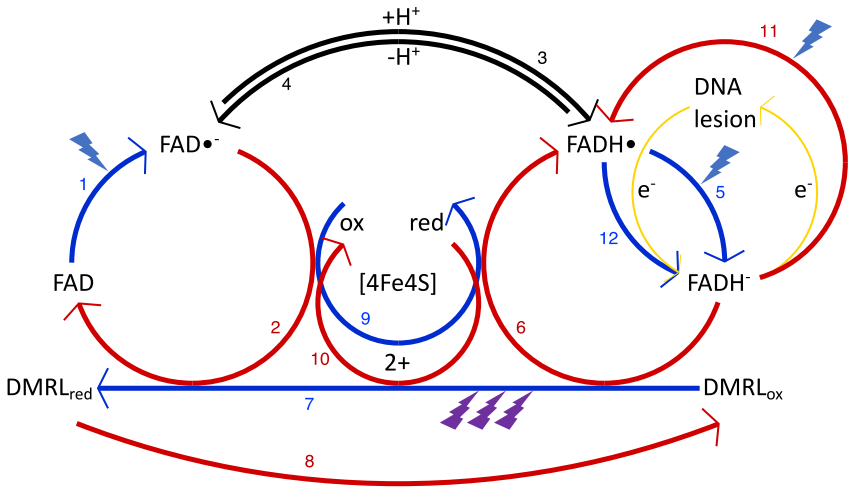

Figure 5. Reaction scheme of PhrB. Blue and red arrows mark reductions and oxidations, respectively

Each redox step is numbered. Engaged blue and red arrows indicate electron transfer from the oxidation step in red to the coupled reduction step in blue. Two reduction steps, 1 and 5, of the flavin in our *in vitro* experiments are light dependent, but they may not be light dependent *in vivo* under a reducing condition. They are not coupled with any oxidation step; therefore, they would require an external electron source, likely the solvent. The redox state of [4Fe4S] could range from 0 to 4+ in principle. However, it cannot be resolved from our spectroscopic data which redox states are involved. Black arrows 3 and 4 mark acid-base reactions that involve proton transfers. The upper right circle marked by 11 and 12 indicates "a photon-powered cyclic electron transfer" in yellow arrows during DNA repair.[3,4]

Such variability is also observed in the raw difference spectra from power titration experiments (Figures 2C and S7) and becomes more evident in time series from PhrB crystals without a reducing agent (Figure S9A). The fifth component, $U_5(\lambda)$, with a broad absorption gain in mid- and near UV, <400 nm (Figure 3B), also displays large fluctuations in the associated coefficient $c_5(t)$ even during the same time series (Figure S8B, right column). Under high-power illumination, some time series exhibit runaway increases along both dimensions of $c_3(t)$ and $c_5(t)$ (Figures 4C, 4D, S10, and S13). In contrast, both $U_3(\lambda)$ and $U_5(\lambda)$ components are barely present in the time series obtained under blue light, where the DMRL absorption is minimal, and in those from the I51W mutant without DMRL, despite the most intense excitation power density (Figures 2D, 2E, S11, and S12). At the same time, phase II of the photoreduction due to DMRL is barely visible in these time series.

We attribute both $U_3(\lambda)$ and $U_5(\lambda)$ spectral components to the spectral changes in [4Fe4S] for the following reasons. First, these components differ from the established spectral features of flavin and DMRL and do not show a biphasic time dependency. Second, their main absorption features generally fall into the mid- to near-UV region reported for protein-bound [4Fe4S] (Figure S4C), although the spectral signatures of the specific valences remain largely uncharacterized.[23–31] Third, we have examined a PhrB mutant, Y391W, that has lost both FAD and DMRL cofactors but retained the [4Fe4S] cluster as the only cofactor.[32] The spectral changes of Y391W arising from chemical oxidation of [4Fe4S] are largely consistent with the absorbance changes in the mid- to near-UV region shown in $U_3(\lambda)$ and $U_5(\lambda)$ in PhrB (Figure S14).

Consistent with what was previously known, [4Fe4S] does not seem to be the main electron source for the FAD photoreduction. First, the [4Fe4S] signals only appear

later in a time series or under high-power illumination following the FAD photoreduction. Second, the behavior of phase I directly depends on whether electrons are abundantly available in the solvent. In the presence of a reducing agent, phase I, that is, FAD photoreduction, appears to proceed more to completion before entering phase II (Figures 4A and 4B). It is likely that the triad of Trp342-Trp390-Tyr391, as previously suggested, offers a pathway to supply electrons from the solvent to FAD instead of gaining electrons from [4Fe4S].[10,32]

However, [4Fe4S] seems to be coupled to the flavin when it is oxidized. When Tyr430 located between [4Fe4S] and FAD is substituted by a Phe residue,[10,14] the time series from the Y430F mutant no longer follow the biphasic path for the $U_1(\lambda)$ and $U_2(\lambda)$ components (Figure 4D). Instead, we observe a straight trajectory in the $c_1(t)$-$c_2(t)$ plot, bypassing the sharp turn dividing phases I and II, suggesting that $U_1(\lambda)$ and $U_2(\lambda)$ increase simultaneously, as if phase I and phase II are synchronized. If the electron transfer between the flavin and [4Fe4S] were indeed disrupted in the Y430F mutant, the oxidation steps of the flavin would be decoupled from [4Fe4S] (step 9 disengaged from steps 2 and 6 in Figure 5), so that [4Fe4S] would no longer receive electrons from the flavin. Therefore, the flavin oxidation steps would be hindered (steps 2 and 6 in Figure 5), and the reduced species of flavin would be enriched. Those electrons used to transfer to [4Fe4S] in the wild type would now promote the photoreduction of DMRL in Y430F (step 7 in Figure 5). Here, we observe synchronized increases of $c_1(t)$ and $c_2(t)$ in a straight line (Figure 4D), which is consistent with electron transfer from flavin to [4Fe4S] through Tyr430 in the wild type. Under high-light conditions, runaway oxidation of [4Fe4S] is possible, as observed from the Y430F mutant (Figures 2F, 4D, and S13) since electrons could be extracted by DMRL but not replenished from the flavin. The altered reaction trajectory of the Y430F mutant seems to suggest that Tyr430 indeed plays a role in electron transfer from flavin to [4Fe4S], but Phe430 would be less effective. However, these electron transfer pathways in PhrB, or more likely a complex network with and without a DNA substrate, are yet to be mapped out.

These observations suggest that the iron-sulfur cluster is coupled to both the oxidation of the flavin and the photoreduction of DMRL as a buffer and a source of electrons whenever needed, that is, an electron cache (Figure 5). However, [4Fe4S] is not the major source of electrons during photoreduction of FAD.

Roles of second chromophore in photolyases

Many photolyases contain a second chromophore located ~10 Å away from the catalytic FAD.[2,33–35] For example, bacterial photolyases have 5,10-methenytetrahydrofolate (MTHF) and flavin mononucleotide (FMN), while photolyases from cyanobacteria, algae, and insects contain 8-HDF (Figure S3). PhrB, a bacterial 6-4 photolyase, features DMRL as the second chromophore. These auxiliary pigments have been long thought to function as antennae that either enhance the light-harvesting efficiency or fill the absorption gap of FAD. This is achieved via a Förster resonance energy transfer (FRET) process in which the excitation energy absorbed by the antenna chromophore is transferred to FAD owing to the spectral overlap between the fluorescence emission of the second chromophore and the absorption of $FADH^-$.

In this work, we observed a hitherto unknown process in which the flavin oxidation and the ribolumazine photoreduction are strongly coupled in the light-induced redox response of PhrB under intense light (Figure 5). Instead of producing more reduced flavin species, a prolonged illumination under violet light reverts flavin to

its fully oxidized form, which is concurrent with the photoreduction of DMRL. This coupling between DMRL and FAD suggests an active role of DMRL beyond the presumed light harvesting. In a typical DNA repair reaction catalyzed by photolyases, it takes less than a nanosecond to transfer an electron from the photoexcited species $FADH^{-}$* to the DNA lesion.[16,36] This rapid electron transfer competes advantageously with other nonproductive pathways, such as fluorescence, that would dissipate the absorbed photon energy. On the other hand, the highly reactive flavin species $FADH^{-}$ could be harmful to the enzyme and/or its substrate DNA when produced in abundance under intense light or continuous illumination. We propose that the DMRL photoreduction offers an effective quenching mechanism for the highly reactive flavin species $FADH^{-}$ via oxidation to revert to the catalytically incompetent FAD. However, it remains to be seen whether this coupling phenomenon is still present in PhrB complexed with the DNA substrates. Nevertheless, this observation has raised an important question whether the equivalent second chromophore in other photolyases, such as 8-HDF, also plays a similar photoprotective role beyond its proposed antenna functions.

Roles of [4Fe4S] in PhrB and other DNA-processing enzymes

Unlike most members of the photolyase/cryptochrome superfamily, PhrB features a [4Fe4S] cluster as the third cofactor. Strikingly, the dispositions of the catalytic FAD and [4Fe4S] in PhrB are highly comparable to those of their counterparts in the [4Fe4S]-containing human DNA primase (Figure S15). In fact, [4Fe4S] has been found in many DNA-processing enzymes, including human DNA polymerases and DNA repair enzymes, suggesting a possible role of [4Fe4S] in redox signaling.[37] However, the molecular mechanism of [4Fe4S] as a redox switch remains elusive because it is experimentally challenging to directly provoke and probe the valence changes and redox responses in [4Fe4S].

Mössbauer spectroscopy studies showed that the [4Fe4S] cluster assumes the 2+ valence in the resting state of PhrB.[38] In principle, [4Fe4S] has five valence states, from 0 to 4+. Such a large redox capacity of four electrons makes [4Fe4S] an ideal electron cache that transiently absorbs excess electrons and supplies them back as needed. However, this is not to say that these five valence states can be easily observed in a steady-state PhrB. Although the spectral signatures have not been established for all five valence states of [4Fe4S], our global analysis identified two significant and independent components, $U_3(\lambda)$ and $U_5(\lambda)$, that describe the observed spectral changes in the mid- to near-UV region, where the [4Fe4S] absorbance is expected. It is highly plausible that the action of [4Fe4S] may transiently involve redox states beyond 2+ and 3+.

We propose that the iron-sulfur cluster serves as an electron buffer or cache that balances the photochemical reactions of FAD and DMRL in PhrB (Figure 5). While $U_3(\lambda)$ is highly susceptible to redox changes introduced by experimental conditions, $U_5(\lambda)$ exhibits fluctuating coefficients around 0, suggesting some "give-and-take" events, as if PhrB is able to self-adjust electron shortage and surplus on the fly under illumination. As Tyr430 is located in between the flavin and [4Fe4S], the single mutant Y430F seems to disrupt the electron transfer route between them. The resulting accumulation of the reduced flavin species thereby triggers an early onset of the DMRL photoreduction (Figure 5). Furthermore, the runaway increases in both $c_3(t)$ and $c_5(t)$ coefficients under high-light conditions indicate that [4Fe4S] may have exceeded its self-adjusting capacity and must be losing more electrons than usual as the light-driven DMRL photoreduction reaches a high level (Figures 2A, 2F, 4C, 4D, and S8B).

Reaction scheme and interplay between three redox cofactors

In the PhrB structure, the catalytic cofactor FAD is about 10 and 15 Å away from DMRL and [4Fe4S], respectively (Figure 1A). The findings of this work suggest that light-induced redox responses of PhrB involve all three cofactors, which constitute an interconnected network within the protein framework. We thus propose a reaction scheme to account for the observed interplay between them (Figure 5). The forward reaction is driven by the FAD photoreduction (depicted by $U_1(\lambda)$), leading to a fully reduced flavin species catalytically competent for DNA repair. Under high-light conditions or prolonged illumination, the DMRL photoreduction kicks in to regulate the reactive species of flavin by actively reverting the highly energetic flavin species to its fully oxidized, inactive state (depicted by $U_2(\lambda)$). Although the exact pathway from the flavin to ribolumazine is not known, this electron transfer process may be mediated by Tyr399 located between FAD and DMRL, 6 and 4 Å away from them, respectively. Meanwhile, our data analysis shows that at least two significant components, $U_3(\lambda)$ and $U_5(\lambda)$, are required to depict the absorption changes associated with [4Fe4S], suggesting that the [4Fe4S] cluster may reach redox states beyond the valences of 2+ and 3+ commonly observed in the steady state. We propose that the [4Fe4S] cluster functions as a high-capacity electron cache by transiently switching between different valence states in response to fluctuations in redox activities of PhrB under different light conditions. When electron supply becomes excessive or exhausted, [4Fe4S] smooths out the spiky electronic potentials via spontaneous reduction or oxidation on the fly. We posit that such coordinated interplay between three redox cofactors is important for a more robust performance of PhrB under different light intensities and wavelength compositions. Of course, it remains to be seen whether these cofactors show similar redox responses in the presence of substrates carrying DNA lesions. Also, exact electron transfer pathways between these cofactors are yet to be mapped out in the PhrB structure.

In summary, this work presents experimental and analytical strategies that allow us to interrogate and dissect the light-induced responses in three redox cofactors of a [4Fe4S]-containing photolyase, PhrB. Using SVD-based joint analyses of 159 time series collected under different light and redox conditions, we were able to deconvolute the spectral features of each cofactor and follow their changes during the light-induced processes in both solution and single crystals. Our findings not only reveal the intricate interplay among the three cofactors in an interconnected redox network within the protein moiety, but also shed light on the hitherto unknown roles of DMRL and [4Fe4S] in regulating concurrent photochemical reactions critical for light-dependent DNA repair functions of photolyases.

EXPERIMENTAL PROCEDURES

Resource availability

Lead contact

All requests should be directed to, and will be fulfilled by, the lead contact, Zhong Ren (zren@uic.edu).

Materials availability

This work did not generate any new, unique substances.

Data and code availability

All data are available within the study and supplemental items. Any requests for additional data will be fulfilled by the lead contact upon reasonable request.

Summary of materials and resources

All PhrB protein samples, including wild type and mutants I51W, Y391W, and Y430F, were expressed and purified as previously described.[8,10,32] Crystallization of wild-type and mutant PhrB followed the published protocols based the hanging-drop vapor-diffusion method.[9,14] The following software packages were used in this work: CCP4, Gnuplot, NumPy, PyMOL, Python, and SciPy.

Absorbance measurement of PhrB solution and single crystals

A sheet of PhrB solution of 5 mg/mL was sandwiched between two quartz glass plates. A shim of 0.5 mm in thickness determined the optical pathlength through the solution sheet. A sheet of buffer solution was also loaded in the same device for measurement of the reference spectrum. A single crystal of PhrB was mounted between the quartz glass plates with the mother liquor. A typical crystal size was about 100 μm in thickness. But the crystal size could vary. Absorption spectra of PhrB in solution and single crystals were measured by an Ocean Optics spectrometer QE Pro with a deuterium-halogen light source (DH-2000-BAL; Ocean Insight). This experimental setup covered a spectral range from mid-UV to near infrared (IR) (200–1,000 nm).

Timing controls of the light sources and the spectrometer (Figure 1F) were programmed via the versatile general-purpose input-output (GPIO) of a Raspberry Pi microcomputer (Raspberry Pi Foundation).

Laser light emitted from two laser diodes, L405P150 and L450P1600MM (Thorlabs), was collimated by an aspherical lens (Thorlabs). PhrB solution and single crystals were pumped by collimated violet light at 405 nm and blue light at 450 nm. Power densities of the pump light at various current settings (Figure 1E) were measured by an optical power meter (PM100USB; Thorlabs). Under the electric current setting of 100 mA through the laser diode, the measured illumination power density was 18 mW/mm^2. This power density was used as a reference in a temporal normalization to calibrate measurements under other power densities (supplemental experimental procedures; Figures S5 and S6). The power density of 1 mW/mm^2 equals 1 sun of 1 kW/m^2, roughly the power density of the solar irradiation on the surface of the earth. The power density of 1 mW/mm^2 requires violet photons of 3.39 $nmol/mm^2$ s at 405 nm or blue photons of 3.76 $nmol/mm^2$ s at 450 nm. The power density around 1 sun for excitation used in our experiments was far weaker than that usually measured in units of GW/cm^2, where 1 $GW/cm^2 = 10^{10}$ sun.

SUPPLEMENTAL INFORMATION

Supplemental information can be found online at https://doi.org/10.1016/j.xcrp.2023.101297.

ACKNOWLEDGMENTS

This work is supported by grants from the University of Illinois at Chicago, National Institutes of Health (R01EY024363), and National Science Foundation (MCB 2017274) to X.Y. This work is also supported by grants from the Deutsche Forschungsgemeinschaft to T.L. (LA 799/7-3) and N.K. (KR 2034/1).

AUTHOR CONTRIBUTIONS

Z.R. and X.Y. conceptualized the research, designed the experiments, and wrote the manuscript. W.K., S.G., and K.B. prepared the protein and crystals. Z.R. collected and analyzed the data. K.T. and G.K. conducted experiments on the Y391W mutant.

X.Y. supervised the work at UIC. N.K. and T.L. supervised the work at KIT. Z.R., X.Y., N.K., and T.L. revised the manuscript.

DECLARATION OF INTERESTS

The authors declare no competing interests.

Received: August 17, 2022
Revised: December 7, 2022
Accepted: January 27, 2023
Published: February 16, 2023

REFERENCES

1. Sinha, R.P., and Häder, D.P. (2002). UV-induced DNA damage and repair: a review. Photochem. Photobiol. Sci. *1*, 225–236. https://doi.org/10.1039/b201230h.

2. Kavakli, I.H., Ozturk, N., and Gul, S. (2019). DNA repair by photolyases. In Advances in Protein Chemistry and Structural Biology (Elsevier), pp. 1–19. https://doi.org/10.1016/bs.apcsb.2018.10.003.

3. Sancar, A. (2003). Structure and function of DNA photolyase and cryptochrome blue-light photoreceptors. Chem. Rev. *103*, 2203–2237. https://doi.org/10.1021/cr0204348.

4. Zhang, M., Wang, L., and Zhong, D. (2017). Photolyase: dynamics and electron-transfer mechanisms of DNA repair. Arch. Biochem. Biophys. *632*, 158–174. https://doi.org/10.1016/j.abb.2017.08.007.

5. Dikbas, U.M., Tardu, M., Canturk, A., Gul, S., Ozcelik, G., Baris, I., Ozturk, N., and Kavakli, I.H. (2019). Identification and characterization of a new class of (6–4) photolyase from Vibrio cholerae. Biochemistry *58*, 4352–4360. https://doi.org/10.1021/acs.biochem.9b00766.

6. Geisselbrecht, Y., Frühwirth, S., Schroeder, C., Pierik, A.J., Klug, G., and Essen, L.O. (2012). CryB from Rhodobacter sphaeroides: a unique class of cryptochromes with new cofactors. EMBO Rep. *13*, 223–229. https://doi.org/10.1038/embor.2012.2.

7. Marizcurrena, J.J., Lamparter, T., and Castro-Sowinski, S. (2020). A (6-4)-photolyase from the Antarctic bacterium Sphingomonas sp. UV9: recombinant production and in silico features. Extremophiles *24*, 887–896. https://doi.org/10.1007/s00792-020-01202-z.

8. Oberpichler, I., Pierik, A.J., Wesslowski, J., Pokorny, R., Rosen, R., Vugman, M., Zhang, F., Neubauer, O., Ron, E.Z., Batschauer, A., and Lamparter, T. (2011). A photolyase-like protein from Agrobacterium tumefaciens with an iron-sulfur cluster. PLoS One *6*, e26775. https://doi.org/10.1371/journal.pone.0026775.

9. Zhang, F., Scheerer, P., Oberpichler, I., Lamparter, T., and Krauß, N. (2013). Crystal structure of a prokaryotic (6-4) photolyase with an Fe-S cluster and a 6,7-dimethyl-8-ribityllumazine antenna chromophore. Proc. Natl. Acad. Sci. USA *110*, 7217–7222. https://doi.org/10.1073/pnas.1302377110.

10. Graf, D., Wesslowski, J., Ma, H., Scheerer, P., Krauß, N., Oberpichler, I., Zhang, F., and Lamparter, T. (2015). Key amino acids in the bacterial (6-4) photolyase PhrB from Agrobacterium fabrum. PLoS One *10*, e0140955. https://doi.org/10.1371/journal.pone.0140955.

11. Liao, D.-I., Wawrzak, Z., Calabrese, J.C., Viitanen, P.V., and Jordan, D.B. (2001). Crystal structure of riboflavin synthase. Structure *9*, 399–408. https://doi.org/10.1016/S0969-2126(01)00600-1.

12. Plaut, G.W.E. (1963). Studies on the nature of the enzymic conversion of 6,7-dimethyl-8-ribityllumazine to riboflavin. J. Biol. Chem. *238*, 2225–2243. https://doi.org/10.1016/S0021-9258(18)67964-5.

13. Scheerer, P., Zhang, F., Kalms, J., von Stetten, D., Krauß, N., Oberpichler, I., and Lamparter, T. (2015). The class III cyclobutane pyrimidine dimer photolyase structure reveals a new antenna chromophore binding site and alternative photoreduction pathways. J. Biol. Chem. *290*, 11504–11514. https://doi.org/10.1074/jbc.M115.637868.

14. Zhang, F., Ma, H., Bowatte, K., Kwiatkowski, D., Mittmann, E., Qasem, H., Krauß, N., Zeng, X., Ren, Z., Scheerer, P., et al. (2017). Crystal structures of bacterial (6-4) photolyase mutants with impaired DNA repair activity. Photochem. Photobiol. *93*, 304–314. https://doi.org/10.1111/php.12699.

15. Thiagarajan, V., Byrdin, M., Eker, A.P.M., Müller, P., and Brettel, K. (2011). Kinetics of cyclobutane thymine dimer splitting by DNA photolyase directly monitored in the UV. Proc. Natl. Acad. Sci. USA *108*, 9402–9407. https://doi.org/10.1073/pnas.1101026108.

16. Zhang, M., Wang, L., Shu, S., Sancar, A., and Zhong, D. (2016). Bifurcating electron-transfer pathways in DNA photolyases determine the repair quantum yield. Science *354*, 209–213. https://doi.org/10.1126/science.aah6071.

17. Henry, E.R., and Hofrichter, J. (1992). Singular value decomposition: application to analysis of experimental data. In Numerical Computer Methods (Academic Press), pp. 129–192.

18. Kawabe, Y., Yoshikawa, T., Chida, T., Tada, K., Kawamoto, M., Fujihara, T., Sassa, T., and Tsutsumi, N. (2015). In Absorption spectrum analysis based on singular value decomposition for photoisomerization and photodegradation in organic dyes, D. Burgess, G. Owen, H. Rana, R. Zamboni, F. Kajzar, and A.A. Szep, eds., p. 96520V. https://doi.org/10.1117/12.2194404.

19. Ren, Z. (2016). Molecular events during translocation and proofreading extracted from 200 static structures of DNA polymerase. Nucleic Acids Res. *44*, 7457–7474. https://doi.org/10.1093/nar/gkw555.

20. Ren, Z. (2019). Ultrafast structural changes decomposed from serial crystallographic data. J. Phys. Chem. Lett. *10*, 7148–7163. https://doi.org/10.1021/acs.jpclett.9b02375.

21. Ren, Z. (2022). Photoinduced isomerization sampling of retinal in bacteriorhodopsin. PNAS Nexus *1*, pgac103. https://doi.org/10.1093/pnasnexus/pgac103.

22. Paulus, B., Illarionov, B., Nohr, D., Roellinger, G., Kacprzak, S., Fischer, M., Weber, S., Bacher, A., and Schleicher, E. (2014). One protein, two chromophores: comparative spectroscopic characterization of 6,7-dimethyl-8-ribityllumazine and riboflavin bound to lumazine protein. J. Phys. Chem. B *118*, 13092–13105. https://doi.org/10.1021/jp507618f.

23. Bartels, P.L., Stodola, J.L., Burgers, P.M.J., and Barton, J.K. (2017). A redox role for the [4Fe4S] cluster of yeast DNA polymerase δ. J. Am. Chem. Soc. *139*, 18339–18348. https://doi.org/10.1021/jacs.7b10284.

24. Grabarczyk, D.B., Ash, P.A., Myers, W.K., Dodd, E.L., and Vincent, K.A. (2019). Dioxygen controls the nitrosylation reactions of a protein-bound [4Fe4S] cluster. Dalton Trans. *48*, 13960–13970. https://doi.org/10.1039/C9DT00924H.

25. O'Brien, E., Holt, M.E., Thompson, M.K., Salay, L.E., Ehlinger, A.C., Chazin, W.J., and Barton, J.K. (2017). The [4Fe4S] cluster of human DNA primase functions as a redox switch using DNA charge transport. Science *355*, eaag1789. https://doi.org/10.1126/science.aag1789.

26. Zeng, J., Geng, M., Jiang, H., Liu, Y., Liu, J., and Qiu, G. (2007). The IscA from Acidithiobacillus ferrooxidans is an iron–sulfur protein which assemble the [Fe4S4] cluster with intracellular iron and sulfur. Arch. Biochem. Biophys. *463*, 237–244. https://doi.org/10.1016/j.abb.2007.03.024.

27. Agarwalla, S., Stroud, R.M., and Gaffney, B.J. (2004). Redox reactions of the iron-sulfur cluster in a ribosomal RNA methyltransferase, RumA: optical and EPR studies. J. Biol. Chem. *279*, 34123–34129. https://doi.org/10.1074/jbc.M405702200.

28. Raulfs, E.C., O'Carroll, I.P., Dos Santos, P.C., Unciuleac, M.-C., and Dean, D.R. (2008). *In vivo* iron–sulfur cluster formation. Proc. Natl. Acad.

Sci. USA *105*, 8591–8596. https://doi.org/10.1073/pnas.0803173105.

29. Wang, W., Huang, H., Tan, G., Si, F., Liu, M., Landry, A.P., Lu, J., and Ding, H. (2010). In vivo evidence for the iron-binding activity of an iron–sulfur cluster assembly protein IscA in Escherichia coli. Biochem. J. *432*, 429–436. https://doi.org/10.1042/BJ20101507.

30. Mapolelo, D.T., Zhang, B., Naik, S.G., Huynh, B.H., and Johnson, M.K. (2012). Spectroscopic and functional characterization of iron–sulfur cluster-bound forms of *Azotobacter vinelandii* ^{Nif}IscA. Biochemistry *51*, 8071–8084. https://doi.org/10.1021/bi3006658.

31. Qian, L., Zheng, C., and Liu, J. (2013). Characterization of iron-sulfur cluster assembly protein isca from Acidithiobacillus ferrooxidans. Biochemistry *78*, 244–251. https://doi.org/10.1134/S000629791303005X.

32. Holub, D., Ma, H., Krauß, N., Lamparter, T., Elstner, M., and Gillet, N. (2018). Functional role of an unusual tyrosine residue in the electron transfer chain of a prokaryotic (6–4) photolyase. Chem. Sci. *9*, 1259–1272. https://doi.org/10.1039/C7SC03386A.

33. Klar, T., Kaiser, G., Hennecke, U., Carell, T., Batschauer, A., and Essen, L.-O. (2006). Natural and non-natural antenna chromophores in the DNA photolyase from Thermus thermophilus. Chembiochem *7*, 1798–1806. https://doi.org/10.1002/cbic.200600206.

34. Park, H.-W., Kim, S.-T., Sancar, A., and Deisenhofer, J. (1995). Crystal structure of DNA photolyase from Escherichia coli. Science *268*, 1866–1872. https://doi.org/10.1126/science.7604260.

35. Tamada, T., Kitadokoro, K., Higuchi, Y., Inaka, K., Yasui, A., de Ruiter, P.E., Eker, A.P., and Miki, K. (1997). Crystal structure of DMA photolyase from Anacystis nidulans. Nat. Struct. Biol. *4*, 887–891. https://doi.org/10.1038/nsb1197-887.

36. Liu, Z., Tan, C., Guo, X., Kao, Y.-T., Li, J., Wang, L., Sancar, A., and Zhong, D. (2011). Dynamics and mechanism of cyclobutane pyrimidine dimer repair by DNA photolyase. Proc. Natl. Acad. Sci. USA *108*, 14831–14836. https://doi.org/10.1073/pnas.1110927108.

37. Barton, J.K., Silva, R.M.B., and O'Brien, E. (2019). Redox chemistry in the genome: emergence of the [4Fe4S] cofactor in repair and replication. Annu. Rev. Biochem. *88*, 163–190. https://doi.org/10.1146/annurev-biochem-013118-110644.

38. Bauer, T.O., Graf, D., Lamparter, T., and Schünemann, V. (2014). Characterization of the photolyase-like iron sulfur protein PhrB from Agrobacterium tumefaciens by Mössbauer spectroscopy. Hyperfine Interact. *226*, 445–449. https://doi.org/10.1007/s10751-013-0969-4.

39. Liu, B., Liu, H., Zhong, D., and Lin, C. (2010). Searching for a photocycle of the cryptochrome photoreceptors. Curr. Opin. Plant Biol. *13*, 578–586. https://doi.org/10.1016/j.pbi.2010.09.005.